



Belle Preprint 2002-18
KEK Preprint 2002-59

Study of $B \rightarrow \rho\pi$ decays at Belle

Belle Collaboration

A. Gordon^u, Y. Chao^z, K. Abe^h, K. Abe^{aq}, N. Abe^{at},
R. Abe^{ac}, T. Abe^{ar}, Byoung Sup Ahn^o, H. Aihara^{as},
M. Akatsu^v, Y. Asano^{ay}, T. Aso^{aw}, V. Aulchenko^b,
T. Aushev^l, A. M. Bakich^{an}, Y. Ban^{ag}, A. Bay^r, I. Bedny^b,
P. K. Behera^{az}, I. Bizjak^m, A. Bondar^b, A. Bozek^{aa},
M. Bračko^{t,m}, T. E. Browder^g, B. C. K. Casey^g,
M.-C. Chang^z, P. Chang^z, B. G. Cheon^{am}, R. Chistov^l,
Y. Choi^{am}, Y. K. Choi^{am}, M. Danilov^l, L. Y. Dong^j,
J. Dragic^u, A. Drutskoy^l, S. Eidelman^b, V. Eiges^l, Y. Enari^v,
C. W. Everton^u, F. Fang^g, H. Fujii^h, C. Fukunaga^{au},
N. Gabyshev^h, A. Garmash^{b,h}, T. Gershon^h, B. Golob^{s,m},
R. Guo^x, J. Haba^h, T. Hara^{ae}, Y. Harada^{ac}, N. C. Hastings^u,
H. Hayashii^w, M. Hazumi^h, E. M. Heenan^u, I. Higuchi^{ar},
T. Higuchi^{as}, L. Hinz^r, T. Hokuue^v, Y. Hoshi^{aq}, S. R. Hou^z,
W.-S. Hou^z, S.-C. Hsu^z, H.-C. Huang^z, T. Igaki^v, Y. Igarashi^h,
T. Iijima^v, K. Inami^v, A. Ishikawa^v, H. Ishino^{at}, R. Itoh^h,
H. Iwasaki^h, Y. Iwasaki^h, H. K. Jang^{al}, J. H. Kang^{bc},
J. S. Kang^o, N. Katayama^h, Y. Kawakami^v, N. Kawamura^a,
T. Kawasaki^{ac}, H. Kichimi^h, D. W. Kim^{am}, Heejong Kim^{bc},
H. J. Kim^{bc}, H. O. Kim^{am}, Hyunwoo Kim^o, S. K. Kim^{al},
T. H. Kim^{bc}, K. Kinoshita^e, S. Korpar^{t,m}, P. Krokovny^b,
R. Kulasiri^e, S. Kumar^{af}, A. Kuzmin^b, Y.-J. Kwon^{bc},
J. S. Lange^{f,ai}, G. Leder^k, S. H. Lee^{al}, J. Li^{ak}, A. Limosani^u,

arXiv:hep-ex/0207007v1 1 Jul 2002

D. Liventsev^ℓ, R.-S. Lu^z, J. MacNaughton^k, G. Majumder^{ao},
 F. Mandl^k, D. Marlow^{ah}, S. Matsumoto^d, T. Matsumoto^{au},
 W. Mitaroff^k, K. Miyabayashi^w, Y. Miyabayashi^v,
 H. Miyake^{ae}, H. Miyata^{ac}, G. R. Moloney^u, T. Mori^d,
 T. Nagamine^{ar}, Y. Nagasakaⁱ, T. Nakadaira^{as}, E. Nakano^{ad},
 M. Nakao^h, J. W. Nam^{am}, Z. Natkaniec^{aa}, K. Neichi^{aq},
 S. Nishida^p, O. Nitoh^{av}, S. Noguchi^w, T. Nozaki^h, S. Ogawa^{ap},
 T. Ohshima^v, T. Okabe^v, S. Okunoⁿ, S. L. Olsen^g, Y. Onuki^{ac},
 W. Ostrowicz^{aa}, H. Ozaki^h, P. Pakhlov^ℓ, H. Palka^{aa},
 C. W. Park^o, H. Park^q, L. S. Peak^{an}, J.-P. Perroud^r,
 M. Peters^g, L. E. Piilonen^{ba}, J. L. Rodriguez^g, F. J. Ronga^r,
 N. Root^b, M. Rozanska^{aa}, K. Rybicki^{aa}, H. Sagawa^h,
 S. Saitoh^h, Y. Sakai^h, M. Satapathy^{az}, A. Satpathy^{h,e},
 O. Schneider^r, S. Schrenk^e, C. Schwanda^{h,k}, S. Semenov^ℓ,
 K. Senyo^v, R. Seuster^g, M. E. Sevier^u, H. Shibuya^{ap},
 V. Sidorov^b, J. B. Singh^{af}, S. Stanič^{ay,1}, M. Starič^m, A. Sugi^v,
 A. Sugiyama^v, K. Sumisawa^h, T. Sumiyoshi^{au}, K. Suzuki^h,
 S. Suzuki^{bb}, S. Y. Suzuki^h, T. Takahashi^{ad}, F. Takasaki^h,
 K. Tamai^h, N. Tamura^{ac}, J. Tanaka^{as}, M. Tanaka^h,
 G. N. Taylor^u, Y. Teramoto^{ad}, S. Tokuda^v, S. N. Tovey^u,
 T. Tsuboyama^h, T. Tsukamoto^h, S. Uehara^h, K. Ueno^z,
 Y. Unno^c, S. Uno^h, Y. Ushiroda^h, G. Varner^g, K. E. Varvell^{an},
 C. C. Wang^z, C. H. Wang^y, J. G. Wang^{ba}, M.-Z. Wang^z,
 Y. Watanabe^{at}, E. Won^o, B. D. Yabsley^{ba}, Y. Yamada^h,
 A. Yamaguchi^{ar}, Y. Yamashita^{ab}, M. Yamauchi^h, H. Yanai^{ac},
 P. Yeh^z, Y. Yuan^j, Y. Yusa^{ar}, J. Zhang^{ay}, Z. P. Zhang^{ak},
 Y. Zheng^g, and D. Žontar^{ay}

^a*Aomori University, Aomori, Japan*

^b*Budker Institute of Nuclear Physics, Novosibirsk, Russia*

^c*Chiba University, Chiba, Japan*

^d*Chuo University, Tokyo, Japan*

^e*University of Cincinnati, Cincinnati, OH, USA*

^f*University of Frankfurt, Frankfurt, Germany*

^g*University of Hawaii, Honolulu, HI, USA*

^h*High Energy Accelerator Research Organization (KEK), Tsukuba, Japan*

- ⁱ*Hiroshima Institute of Technology, Hiroshima, Japan*
- ^j*Institute of High Energy Physics, Chinese Academy of Sciences, Beijing, PR China*
- ^k*Institute of High Energy Physics, Vienna, Austria*
- ^l*Institute for Theoretical and Experimental Physics, Moscow, Russia*
- ^m*J. Stefan Institute, Ljubljana, Slovenia*
- ⁿ*Kanagawa University, Yokohama, Japan*
- ^o*Korea University, Seoul, South Korea*
- ^p*Kyoto University, Kyoto, Japan*
- ^q*Kyungpook National University, Taegu, South Korea*
- ^r*Institut de Physique des Hautes Énergies, Université de Lausanne, Lausanne, Switzerland*
- ^s*University of Ljubljana, Ljubljana, Slovenia*
- ^t*University of Maribor, Maribor, Slovenia*
- ^u*University of Melbourne, Victoria, Australia*
- ^v*Nagoya University, Nagoya, Japan*
- ^w*Nara Women's University, Nara, Japan*
- ^x*National Kaohsiung Normal University, Kaohsiung, Taiwan*
- ^y*National Lien-Ho Institute of Technology, Miao Li, Taiwan*
- ^z*National Taiwan University, Taipei, Taiwan*
- ^{aa}*H. Niewodniczanski Institute of Nuclear Physics, Krakow, Poland*
- ^{ab}*Nihon Dental College, Niigata, Japan*
- ^{ac}*Niigata University, Niigata, Japan*
- ^{ad}*Osaka City University, Osaka, Japan*
- ^{ae}*Osaka University, Osaka, Japan*
- ^{af}*Panjab University, Chandigarh, India*
- ^{ag}*Peking University, Beijing, PR China*
- ^{ah}*Princeton University, Princeton, NJ, USA*
- ^{ai}*RIKEN BNL Research Center, Brookhaven, NY, USA*
- ^{aj}*Saga University, Saga, Japan*
- ^{ak}*University of Science and Technology of China, Hefei, PR China*
- ^{al}*Seoul National University, Seoul, South Korea*
- ^{am}*Sungkyunkwan University, Suwon, South Korea*
- ^{an}*University of Sydney, Sydney, NSW, Australia*
- ^{ao}*Tata Institute of Fundamental Research, Bombay, India*
- ^{ap}*Toho University, Funabashi, Japan*
- ^{aq}*Tohoku Gakuin University, Tagajo, Japan*

^{ar} *Tohoku University, Sendai, Japan*

^{as} *University of Tokyo, Tokyo, Japan*

^{at} *Tokyo Institute of Technology, Tokyo, Japan*

^{au} *Tokyo Metropolitan University, Tokyo, Japan*

^{av} *Tokyo University of Agriculture and Technology, Tokyo, Japan*

^{aw} *Toyama National College of Maritime Technology, Toyama, Japan*

^{ay} *University of Tsukuba, Tsukuba, Japan*

^{az} *Utkal University, Bhubaneswer, India*

^{ba} *Virginia Polytechnic Institute and State University, Blacksburg, VA, USA*

^{bb} *Yokkaichi University, Yokkaichi, Japan*

^{bc} *Yonsei University, Seoul, South Korea*

Abstract

This paper describes a study of B meson decays to the pseudoscalar-vector final state $\rho\pi$ using 31.9×10^6 $B\bar{B}$ events collected with the Belle detector at KEKB. The branching fractions $\mathcal{B}(B^+ \rightarrow \rho^0\pi^+) = (8.0_{-2.0}^{+2.3+0.7}) \times 10^{-6}$ and $\mathcal{B}(B^0 \rightarrow \rho^\pm\pi^\mp) = (20.8_{-6.3}^{+6.0+2.8}) \times 10^{-6}$ are obtained. In addition, a 90% confidence level upper limit of $\mathcal{B}(B^0 \rightarrow \rho^0\pi^0) < 5.3 \times 10^{-6}$ is reported.

Key words: $\rho\pi$, branching fraction

PACS: 13.25.hw, 14.40.Nd

The decays of B -mesons to pseudoscalar and vector particles provide opportunities for investigating the phenomenon of CP violation. Of particular interest are the quasi-two-body $B \rightarrow \rho\pi$ decays to three-pion final states. These can be used to measure the angles ϕ_2 and ϕ_3 of the unitarity triangle: ϕ_2 can be determined from a full Dalitz plot analysis of the modes $B^0 \rightarrow \rho^\pm\pi^\mp$ and $B^0 \rightarrow \rho^0\pi^0$ [1]; ϕ_3 can be extracted from the interference of $B^+ \rightarrow \chi_{c0}\pi^+$ and $B^+ \rightarrow \rho^0\pi^+$ in $B^+ \rightarrow \pi^+\pi^-\pi^+$ decays [2]. While the data set used here is too small for this type of analysis, it can be used to study the branching fractions of these decays. The ratio of branching fractions $R = \mathcal{B}(B^0 \rightarrow \rho^\pm\pi^\mp)/\mathcal{B}(B^+ \rightarrow \rho^0\pi^+)$ is particularly interesting as theoretical predictions for the value of R vary over a wide range depending on the assumptions made in its calculation [3–8].

In this paper, a search for B meson decays of the type $B \rightarrow \rho\pi$ is described. Both the neutral ($B^0 \rightarrow \rho^\pm\pi^\mp$ and $B^0 \rightarrow \rho^0\pi^0$) and charged ($B^+ \rightarrow \rho^0\pi^+$)

¹ on leave from Nova Gorica Polytechnic, Nova Gorica, Slovenia

modes are examined. Here and throughout the text, inclusion of charge conjugate modes is implied and for the neutral decay, $B^0 \rightarrow \rho^\pm \pi^\mp$, the notation implies a sum over both the modes. The data sample used in this analysis was taken by the Belle detector [9] at KEKB [10], an asymmetric storage ring that collides 8 GeV electrons against 3.5 GeV positrons. This produces $\Upsilon(4S)$ mesons that decay into $B^0 \bar{B}^0$ or $B^+ B^-$ pairs. The data sample has an integrated luminosity of 29.4 fb^{-1} and consists of 31.9×10^6 $B\bar{B}$ pairs.

The Belle detector is a general purpose spectrometer based on a 1.5 T superconducting solenoid magnet. Charged particle tracking is achieved with a three-layer double-sided silicon vertex detector (SVD) surrounded by a central drift chamber (CDC) that consists of 50 layers segmented into 6 axial and 5 stereo super-layers. The CDC covers the polar angle range between 17° and 150° in the laboratory frame, which corresponds to 92% of the full centre of mass (CM) frame solid angle. Together with the SVD, a transverse momentum resolution of $(\sigma_{p_t}/p_t)^2 = (0.0019 p_t)^2 + (0.0030)^2$ is achieved, where p_t is in GeV/c .

Charged hadron identification is provided by a combination of three devices: a system of 1188 aerogel Čerenkov counters (ACC) covering the momentum range 1–3.5 GeV/c , a time-of-flight scintillation counter system (TOF) for track momenta below 1.5 GeV/c , and dE/dx information from the CDC for particles with very low or high momenta. Information from these three devices is combined to give the likelihood of a particle being a kaon, L_K , or pion, L_π . Kaon-pion separation is then accomplished based on the likelihood ratio $L_\pi/(L_\pi + L_K)$. Particles with a likelihood ratio greater than 0.6 are identified as pions. The pion identification efficiencies are measured using a high momentum D^{*+} data sample, where $D^{*+} \rightarrow D^0 \pi^+$ and $D^0 \rightarrow K^- \pi^+$. With this pion selection criterion, the typical efficiency for identifying pions in the momentum region $0.5 \text{ GeV}/c < p < 4 \text{ GeV}/c$ is $(88.5 \pm 0.1)\%$. By comparing the D^{*+} data sample with a Monte Carlo (MC) sample, the systematic error in the particle identification (PID) is estimated to be 1.4% for the mode with three charged tracks and 0.9% for the modes with two.

Surrounding the charged PID devices is an electromagnetic calorimeter (ECL) consisting of 8736 CsI(Tl) crystals with a typical cross-section of $5.5 \times 5.5 \text{ cm}^2$ at the front surface and $16.2 X_0$ in depth. The ECL provides a photon energy resolution of $(\sigma_E/E)^2 = 0.013^2 + (0.0007/E)^2 + (0.008/E^{1/4})^2$, where E is in GeV.

Electron identification is achieved by using a combination of dE/dx measurements in the CDC, the response of the ACC and the position and shape of the electromagnetic shower from the ECL. Further information is obtained from the ratio of the total energy registered in the calorimeter to the particle momentum, E/p_{tab} .

Charged tracks are required to come from the interaction point and have transverse momenta above 100 MeV/ c . Tracks consistent with being an electron are rejected and the remaining tracks must satisfy the pion identification requirement. The performance of the charged track reconstruction is studied using high momentum $\eta \rightarrow \gamma\gamma$ and $\eta \rightarrow \pi^+\pi^-\pi^0$ decays. Based on the relative yields between data and MC, we assign a systematic error of 2% to the single track reconstruction efficiency.

Neutral pion candidates are detected with the ECL via their decay $\pi^0 \rightarrow \gamma\gamma$. The π^0 mass resolution, which is asymmetric and varies slowly with the π^0 energy, averages to $\sigma = 4.9$ MeV/ c^2 . The neutral pion candidates are selected from $\gamma\gamma$ pairs by requiring that their invariant mass to be within 3σ of the nominal π^0 mass.

To reduce combinatorial background, a selection criteria is applied to the photon energies and the π^0 momenta. Photons in the barrel region are required to have energies over 50 MeV, while a 100 MeV requirement is made for photons in the end-cap region. The π^0 candidates are required to have a momentum greater than 200 MeV/ c in the laboratory frame. For π^0 s from $B\bar{B}$ events, the efficiency of these requirements is about 40%. Furthermore, the π^0 helicity, defined as the absolute cosine of the angle between the photon direction in the π^0 rest frame and the π^0 direction in the lab frame, is required to be less than 0.95. The behavior of the π^0 reconstruction efficiency as a function of momentum is studied using $D^{*+} \rightarrow D^0\pi^+$ decays by comparing the relative yields between data and MC in the $D^0 \rightarrow K^-\pi^+\pi^0$ and $K^-\pi^+$ sub-channels. The residual systematic uncertainties are 9.8% for low momentum π^0 s ($p < 500$ MeV/ c) and 7.7% otherwise.

Neutral ρ candidates are reconstructed using the decay $\rho^0 \rightarrow \pi^+\pi^-$ with the invariant mass of the charged pion pair required to be between 0.6 GeV/ c^2 and 0.95 GeV/ c^2 . The decay $\rho^+ \rightarrow \pi^0\pi^+$ is used to reconstruct charged ρ candidates with the invariant mass of the pion pair required to be between 0.62 GeV/ c^2 and 0.92 GeV/ c^2 .

Candidate B mesons are identified by pairing ρ and π candidates that pass the above criteria. The candidates are then selected using the beam-constrained mass $M_{bc} = \sqrt{E_{\text{beam}}^2 - p_B^2}$ and the energy difference $\Delta E = E_B - E_{\text{beam}}$. Here, p_B and E_B are the momentum and energy of a B candidate in the CM frame and E_{beam} is the CM beam energy. An incorrect mass hypothesis for a pion or kaon produces a shift of about 46 MeV in ΔE , providing extra discrimination between these particles. The width of the M_{bc} distributions is primarily due to the beam energy spread and is well modelled with a Gaussian of width 3.3 MeV/ c^2 for the modes with a neutral pion and 2.7 MeV/ c^2 for the mode without. The ΔE distribution is found to be asymmetric with a small tail on the lower side for the modes with a π^0 . This is due to γ interactions with

material in front of the calorimeter and shower leakage out of the calorimeter. The ΔE distribution can be well modelled with a Gaussian when no neutral particles are present. Events with $5.2 \text{ GeV}/c^2 < M_{bc} < 5.3 \text{ GeV}/c^2$ and $|\Delta E| < 0.3 \text{ GeV}$ are selected for the final analysis.

The dominant background comes from continuum $e^+e^- \rightarrow q\bar{q}$ ($q = u, d, s, c$) production. This background is suppressed using variables that quantify the difference in the event topology between spherical $B\bar{B}$ events and jet-like $q\bar{q}$ events. The most powerful suppression is achieved using variables derived from the Fox-Wolfram moments [11] but altered to contain the additional information of whether or not a track comes from the B candidate in the event [12]. These modified moments enhance the discriminating power of the original Fox-Wolfram moments and are defined as

$$R_l = \frac{\sum_{i,k} |p_i||p_k|P_l(\cos\theta_{ik})}{\sum_{i,k} |p_i||p_k|}, \quad r_l = \frac{\sum_{i,j} |p_i||p_j|P_l(\cos\theta_{ij})}{\sum_{i,j} |p_i||p_j|},$$

where p indicates the particle momentum, l runs from 1 to 4 and P_l is the Legendre polynomial of l th order, k runs over the daughters of a B candidate and i and j enumerate photons and charged particles in the event not associated with the B candidate. Since R_1 , R_3 and r_1 are found to be correlated with M_{bc} , they are not used. Another event topology variable used is S_\perp , defined as the scalar sum of the transverse momenta (with respect to the thrust axis) of the particles outside a 45° cone around the thrust axis, divided by the scalar sum of the momenta of all the particles. These variables then are combined to form a Fisher discriminant [13]

$$\mathcal{F} = \sum_{l=2,4} \alpha_l R_l + \sum_{l=2,3,4} \beta_l r_l + \gamma S_\perp,$$

where α_l , β_l and γ are optimized to maximize the separation between signal and continuum events. Also used for continuum suppression is the B flight direction, $\cos\theta_B$, defined as the cosine of the angle the B meson momentum vector makes with the positron beam axis. As $\cos\theta_B$ is uncorrelated with the other continuum suppression variables, it is left out of \mathcal{F} .

Probability density functions (PDFs) are obtained for \mathcal{F} and $\cos\theta_B$ using MC simulations for signal and background. The PDFs are then combined to form a likelihood ratio $\mathcal{L} = \mathcal{L}_s/(\mathcal{L}_s + \mathcal{L}_{q\bar{q}})$, where \mathcal{L}_s and $\mathcal{L}_{q\bar{q}}$ are the product of the signal and background PDFs, respectively. Signal events are selected by requiring that $\mathcal{L} > 0.9$, which has a signal efficiency of about 40% for modes with a π^0 and 35% for the all charged particle mode. The systematic error in the likelihood ratio requirement is determined using a sample of $B^+ \rightarrow \bar{D}^0 \pi^+$ decays. By comparing the yields in data and MC after the likelihood ratio

requirement, the systematic errors are determined to be 4% for the modes with a π^0 and 6% for the mode without.

The final variable used for continuum suppression is the ρ helicity angle, θ_h , defined as the angle between the direction of the decay pion from the ρ in the ρ rest frame and the ρ in the B rest frame. The requirement of $|\cos \theta_h| > 0.3$ is made independently of the likelihood ratio as it is effective in suppressing the background from B decays as well as the $q\bar{q}$ continuum.

Although continuum events are the largest background, the mode with all charged particles has other backgrounds in the signal region from B meson decays. To study this, a large MC sample of $B\bar{B}$ events is used [14]. The largest component of this background is found to come from decays of the type $B \rightarrow D\pi$; when the D meson decays via $D \rightarrow \pi^+\pi^-$, events can directly reach the signal region while the decay $D \rightarrow K^-\pi^+$ can reach the signal region with the kaon misidentified as a pion. Decays with J/ψ and $\psi(2S)$ mesons can also populate the signal region if both the daughter leptons are misidentified as pions. These events are excluded by making requirements on the invariant mass of the intermediate particles: $|M(\pi^+\pi^-) - M_{D^0}| > 0.14$ GeV/ c^2 , $|M(\pi^+\pi^0) - M_{D^+}| > 0.05$ GeV/ c^2 , $|M(\pi^+\pi^-) - M_{J/\psi}| > 0.07$ GeV/ c^2 and $|M(\pi^+\pi^-) - M_{\psi(2S)}| > 0.05$ GeV/ c^2 . The widest cut is made around the D^0 mass to account for the mass shift due to misidentifying the kaons in D^0 decays as pions.

Fig. 1 shows the ΔE and M_{bc} distributions for the three modes analysed after all the selection criteria have been applied. The ΔE and M_{bc} plots are shown for events that lie within 3σ of the nominal M_{bc} and ΔE values, respectively. The signal yields are obtained by performing maximum likelihood fits, each using a single signal function and one or more background functions. The signal functions are obtained from the MC and adjusted based on comparisons of $B^+ \rightarrow \bar{D}^0\pi^+$ decays in the data and MC. All parameters in the signal function are fixed except the overall normalization, which is allowed to float. The final branching fractions are extracted using the ΔE signal yield, as this provides a kinematic separation of the background modes. In calculating the branching fractions, the decay rates of the $\Upsilon(4S)$ into B^+B^- and $B^0\bar{B}^0$ are assumed to be equal.

The M_{bc} distribution for all modes is fitted with a single Gaussian and an ARGUS background function [15]. The normalization of the ARGUS function is left to float and shape of the function is fixed from the ΔE sideband: -0.25 GeV $< \Delta E < -0.08$ GeV and 5.2 GeV/ $c^2 < M_{bc} < 5.3$ GeV/ c^2 . For the mode with only charged pions in the final state, the ΔE distribution is fitted with a single Gaussian for the signal and a linear function with fixed shape for the continuum background. The normalization of the linear function is left to float and the slope is fixed from the M_{bc} sideband, 5.2 GeV/ $c^2 < M_{bc} < 5.26$

GeV/ c^2 , $|\Delta E| < 0.3$ GeV. There are also other rare B decays that are expected to contaminate the ΔE distribution. For the mode without a π^0 , these modes are of the type $B^0 \rightarrow h^+h^-$ (where h denotes a π or K), $B \rightarrow \rho\rho$ (including all combinations of charged and neutral ρ mesons, where the polarizations of the ρ mesons are assumed to be longitudinal) and $B \rightarrow K\pi\pi$ (including the decays $B^+ \rightarrow \rho^0 K^+$, $B^+ \rightarrow K^{*0}\pi^+$, $B^+ \rightarrow K_0^*(1430)^0\pi^+$, $B^+ \rightarrow f_0(980)K^+$ and $B^+ \rightarrow f_0(1370)K^+$) [16]. These background modes are accounted for by using smoothed histograms whose shapes have been determined by combining MC distributions. The three $B \rightarrow \rho\rho$ modes are combined into one histogram. The normalization of this component is allowed to float in the fit due to the uncertainty in the branching fractions of the $B \rightarrow \rho\rho$ modes. Likewise, the $B \rightarrow hh$ and all the $B \rightarrow K\pi\pi$ modes are combined to form one hh and one $K\pi\pi$ component. The normalizations of these components are fixed to their expected yields, which are calculated using efficiencies determined by MC and branching fractions measured by previous Belle analyses [16,17].

The ΔE fits for the modes with a π^0 in the final state have the signal component modelled by a Crystal Ball function [18] to account for the asymmetry in the ΔE distribution. As for the $B^+ \rightarrow \rho^0\pi^+$ mode, the continuum background is modelled by a linear function with fixed slope. Unlike the $B^+ \rightarrow \rho^0\pi^+$ mode, a component is included for the background from the $b \rightarrow c$ transition. The parameterization for rare B decays includes one component for the $B \rightarrow K\pi\pi^0$ modes ($B^0 \rightarrow \rho^+K^-$ and $B^0 \rightarrow K^{*+}\pi^-$) [19] and one for all the $B \rightarrow \rho\rho$ modes. The normalization of the $B \rightarrow \rho\rho$ component is left to float while the other components from B decays are fixed to their expected yields.

Table 1 summarizes the results of the ΔE fits, showing the number of events, signal yields, reconstruction efficiencies, statistical significance and branching fractions or upper limits for each fit. The statistical significance is defined as $\sqrt{-2\ln(\mathcal{L}_0/\mathcal{L}_{max})}$, where \mathcal{L}_{max} denotes the likelihood at the nominal signal yield and \mathcal{L}_0 is the likelihood with the signal yield fixed to zero. For the $\rho^0\pi^+$ and $\rho^+\pi^-$ modes, the yields obtained from the ΔE fit are $24.3_{-6.2}^{+6.9}$ and $44.6_{-13.4}^{+12.8}$, respectively. Both signals have a significance of over 3σ and consistent signal yields are obtained from the M_{bc} distributions. No excess above background is seen in the ΔE fit for the $\rho^0\pi^0$ mode and an excess of 14 ± 6 events is seen in the M_{bc} distribution. The M_{bc} yield has a significance of 2.3σ and may be due to background from rare B decays. An upper limit (UL) is obtained for this mode based on the ΔE yield. The upper limit is calculated using the 90% confidence level UL of the signal yield (N_s), obtained by integrating the likelihood function to be $\int_0^{UL} \mathcal{L}(N_s)dN_s / \int_0^\infty \mathcal{L}(N_s)dN_s = 0.9$, where $\mathcal{L}(N_s)$ denotes the maximum likelihood with the signal yield fixed at N_s .

The systematic errors in the branching fractions are obtained by quadratically summing the systematic uncertainties in the signal yield, tracking, particle identification, π^0 reconstruction and the likelihood ratio requirement. The

systematic error in the fitted signal yield is estimated by independently varying each fixed parameter in the fit by 1σ . The final results are $\mathcal{B}(B^+ \rightarrow \rho^0\pi^+) = (8.0_{-2.0-0.7}^{+2.3+0.7}) \times 10^{-6}$ and $\mathcal{B}(B^0 \rightarrow \rho^\pm\pi^\mp) = (20.8_{-6.3-3.1}^{+6.0+2.8}) \times 10^{-6}$ where the first error is statistical and the second is systematic. For the $\rho^0\pi^0$ mode, one standard deviation of the systematic error is added to the statistical limit to obtain a conservative upper limit at 90% confidence of 5.3×10^{-6} .

The possibility of a nonresonant $B \rightarrow \pi\pi\pi$ background is also examined. To check for this type of background, the M_{bc} and ΔE yields are determined for different $\pi\pi$ invariant mass bins. By fitting the M_{bc} distribution in $\pi\pi$ invariant mass bins with $B \rightarrow \rho\pi$ and $B \rightarrow \pi\pi\pi$ MC distributions, the nonresonant contribution is found to be below 4%. To account for this possible background, errors 3.7% and 3.2% are added in quadrature to the systematic errors of the $\rho^+\pi^-$ and $\rho^0\pi^+$ modes, respectively. The $\pi\pi$ invariant mass distributions are shown in Fig. 2. Two plots are shown for the $\rho^+\pi^-$ and $\rho^0\pi^+$ modes, one with events from the M_{bc} sideband superimposed over the events from the signal region (upper) and one with events from signal MC superimposed over events from the signal region with the sideband subtracted (lower). Fig. 3 shows the distribution of the helicity variable, $\cos\theta_h$, for the two modes with all selection criteria applied except the helicity condition. Events from $\rho\pi$ decays are expected to follow a $\cos^2\theta$ distribution while nonresonant and other background decays have an approximately uniform distribution. The helicity plots are obtained by fitting the M_{bc} distribution in eight helicity bins ranging from -1 to 1 . The M_{bc} yield is then plotted against the helicity bin for each mode and the expected MC signal distributions are superimposed. Both the $\pi\pi$ mass spectrum and the helicity distributions provide evidence that the signal events are consistent with being from $\rho\pi$ decays.

The results obtained here can be used to calculate the ratio of branching fractions $R = \mathcal{B}(B^0 \rightarrow \rho^\pm\pi^\mp)/\mathcal{B}(B^+ \rightarrow \rho^0\pi^+)$, which gives $R = 2.6 \pm 1.0 \pm 0.4$, where the first error is statistical and second is systematic. This is consistent with values obtained by CLEO [20] and BaBar [21,22] as shown in Table 2. Theoretical calculations done at tree level assuming the factorization approximation for the hadronic matrix elements give $R \sim 6$ [3]. Calculations that include penguin contributions, off-shell B^* excited states or additional $\pi\pi$ resonances [4–8] might yield better agreement with the the measured value of R .

In conclusion, statistically significant signals have been observed in the $B \rightarrow \rho\pi$ modes using a $31.9 \times 10^6 B\bar{B}$ event data sample collected with the Belle detector. The branching fractions obtained are $\mathcal{B}(B^+ \rightarrow \rho^0\pi^+) = (8.0_{-2.0-0.7}^{+2.3+0.7}) \times 10^{-6}$ and $\mathcal{B}(B^0 \rightarrow \rho^\pm\pi^\mp) = (20.8_{-6.3-3.1}^{+6.0+2.8}) \times 10^{-6}$ where the first error is statistical and the second is systematic. No evidence was seen for the mode $B^0 \rightarrow \rho^0\pi^0$ and an upper limit of 5.3×10^{-6} at 90% confidence level was obtained.

We wish to thank the KEKB accelerator group for the excellent operation of the KEKB accelerator. We acknowledge support from the Ministry of Education, Culture, Sports, Science, and Technology of Japan and the Japan Society for the Promotion of Science; the Australian Research Council and the Australian Department of Industry, Science and Resources; the National Science Foundation of China under contract No. 10175071; the Department of Science and Technology of India; the BK21 program of the Ministry of Education of Korea and the CHEP SRC program of the Korea Science and Engineering Foundation; the Polish State Committee for Scientific Research under contract No. 2P03B 17017; the Ministry of Science and Technology of the Russian Federation; the Ministry of Education, Science and Sport of the Republic of Slovenia; the National Science Council and the Ministry of Education of Taiwan; and the U.S. Department of Energy.

References

- [1] A.E. Snyder and H.R. Quinn, Phys. Rev. D **48**, 2139 (1993).
- [2] I. Bediaga, R.E. Blanco, C. Göbel, and R. Méndez-Galain, Phys. Rev. Lett. **81**, 4067 (1998).
- [3] M. Bauer, B. Stech, and M. Wirbel, Z. Phys. C **34**, 103 (1987).
- [4] A. Deandrea *et al.*, Phys. Rev. D **62**, 036001 (2000).
- [5] Y.H. Chen, H.Y. Cheng, B. Tseng and K.C. Yang, Phys. Rev. D **60**, 094014 (1999).
- [6] C.D. Lu and M.Z. Yang, Eur. Phys. J C **23**, 275 (2002).
- [7] J. Tandean and S. Gardner, SLAC-PUB-9199; hep-ph/0204147.
- [8] S. Gardner and Ulf-G. Meißner, Phys. Rev. D **65**, 094004 (2002).
- [9] Belle Collaboration, A. Abashian *et al.*, Nucl. Instr. and Meth. A **479**, 117 (2002).
- [10] E. Kikutani ed., KEK Preprint 2001-157 (2001), to appear in Nucl. Instr. and Meth. A.
- [11] G.C. Fox and S. Wolfram, Phys. Rev. Lett. **41**, 1581 (1978).
- [12] This modification of the Fox-Wolfram moments was first proposed in a series of lectures on continuum suppression at KEK by Dr. R. Enomoto in May and June of 1999. For a more detailed description see Belle Collaboration, K. Abe *et al.*, Phys. Lett. B **511**, 151 (2001).
- [13] CLEO Collaboration, D.M. Asner *et al.*, Phys. Rev. D **53**, 1039 (1996).

- [14] These MC events are generated with the CLEO group's QQ program, see <http://www.lns.cornell.edu/public/CLEO/soft/qq>. The detector response is simulated using GEANT, R. Brun *et al.*, GEANT 3.21, CERN Report DD/EE/84-1, 1984.
- [15] The ARGUS Collaboration, H. Albrecht *et al.*, Phys. Lett. B **241**, 278 (1990).
- [16] Belle Collaboration, A. Garmash *et al.*, Phys. Rev. D **65**, 092005 (2002).
- [17] Belle Collaboration, K. Abe *et al.*, Phys. Rev. Lett. **87**, 101801 (2001).
- [18] J.E. Gaiser *et al.*, Phys. Rev. D **34**, 711 (1986).
- [19] Belle Collaboration, K. Abe *et al.*, BELLE-CONF-0115, submitted as a contribution paper to the 2001 International Europhysics Conference on High Energy Physics (EPS-HEP 2001).
- [20] CLEO Collaboration, C.P. Jessop *et al.*, Phys. Rev. Lett. **85**, 2881 (2000).
- [21] Babar Collaboration, B. Aubert *et al.*, submitted as a contribution paper to the 20th International Symposium on Lepton and Photon Interactions at High Energy (LP01); hep-ex/0107058.
- [22] BaBar Collaboration, B. Aubert *et al.*, submitted as a contribution paper to the XXXth International Conference on High Energy Physics (ICHEP2000); hep-ex/0008058.

Table 1

ΔE fit results. Shown for each mode are the number of events in the fit, the signal yield, the reconstruction efficiency, the branching fraction (\mathcal{B}) or 90% confidence level upper limit (UL) and the statistical significance of the fit. The first error in the branching fraction is statistical, the second is systematic.

Channel	Events	Signal Yield	Eff.(%)	$\mathcal{B}/\text{UL}(\times 10^{-6})$	Significance
$\rho^0\pi^+$	154	$24.3^{+6.9}_{-6.2}$	9.6	$8.0^{+2.3+0.7}_{-2.0-0.7}$	4.4σ
$\rho^+\pi^-$	301	$44.6^{+12.8}_{-13.4}$	6.8	$20.8^{+6.0+2.8}_{-6.3-3.1}$	3.7σ
$\rho^0\pi^0$	116	-4.4 ± 8.5	8.5	< 5.3	-

Table 2

A comparison between the results of the Belle, BaBar and CLEO experiments for the $B \rightarrow \rho\pi$ branching fractions and the ratio $R = \mathcal{B}(B^0 \rightarrow \rho^\pm\pi^\mp)/\mathcal{B}(B^+ \rightarrow \rho^0\pi^+)$. The CLEO results come from reference [20]. The BaBar results for $\rho^+\pi^-$ and $\rho^0\pi^+$ come from references [21] and [22], respectively.

Experiment	$\mathcal{B}(B^0 \rightarrow \rho^\pm\pi^\mp) \times 10^{-6}$	$\mathcal{B}(B^+ \rightarrow \rho^0\pi^+) \times 10^{-6}$	R
Belle	$20.8^{+6.0+2.8}_{-6.3-3.1}$	$8.0^{+2.3+0.7}_{-2.0-0.7}$	2.6 ± 1.1
BaBar	$28.9 \pm 5.4 \pm 4.3$	$24 \pm 8 \pm 3$	1.2 ± 0.5
CLEO	$27.6^{+8.4}_{-7.4} \pm 4.2$	$10.4^{+3.3}_{-3.4} \pm 2.1$	2.7 ± 1.3

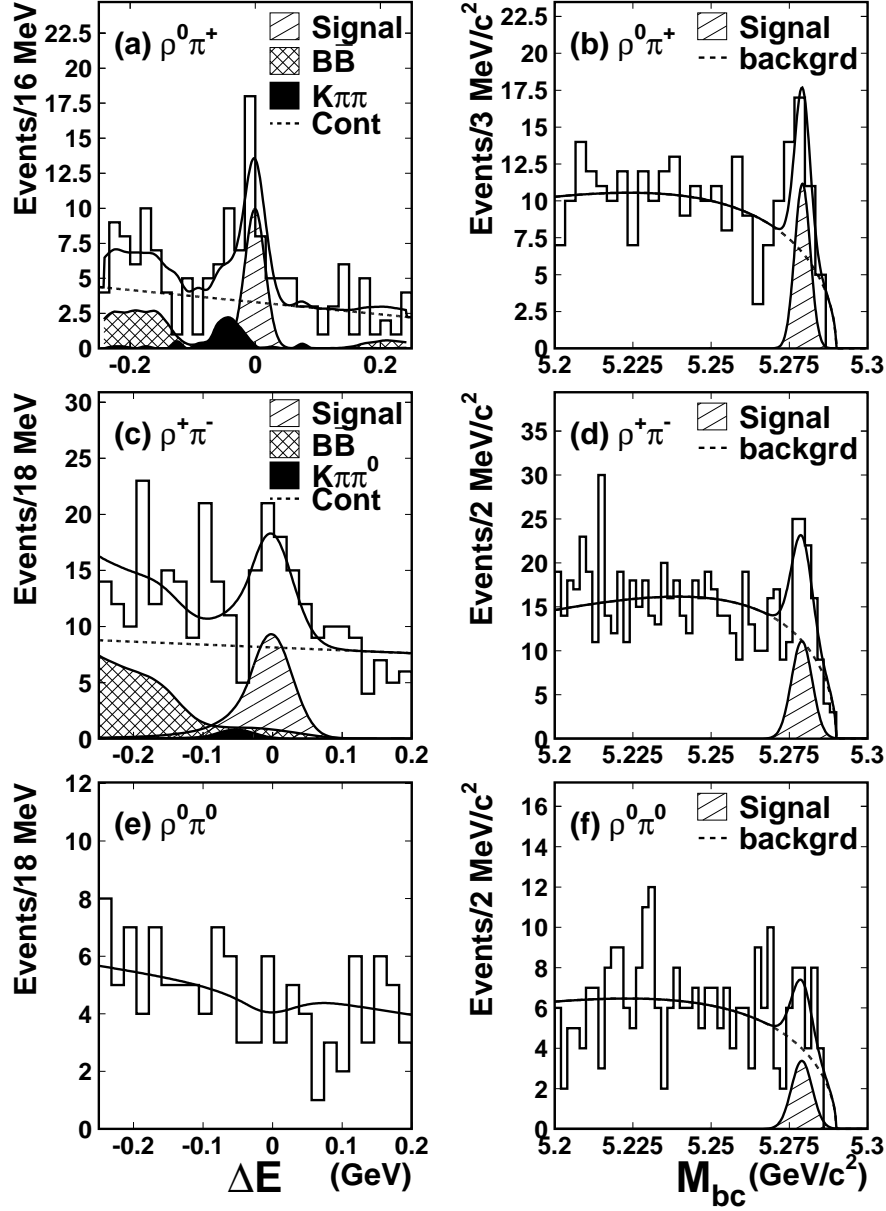


Fig. 1. The ΔE (left) and M_{bc} (right) fits to the three $B \rightarrow \rho\pi$ modes: $\rho^0\pi^+$, $\rho^+\pi^-$ and $\rho^0\pi^0$. The histograms show the data, the solid lines show the total fit and the dashed lines show the continuum component. In (a) the contribution from the $B \rightarrow \rho\rho$ and $B \rightarrow hh$ modes is shown by the cross hatched component. In (c) the cross hatched component shows the contribution from the $b \rightarrow c$ transition and $B \rightarrow \rho\rho$ modes.

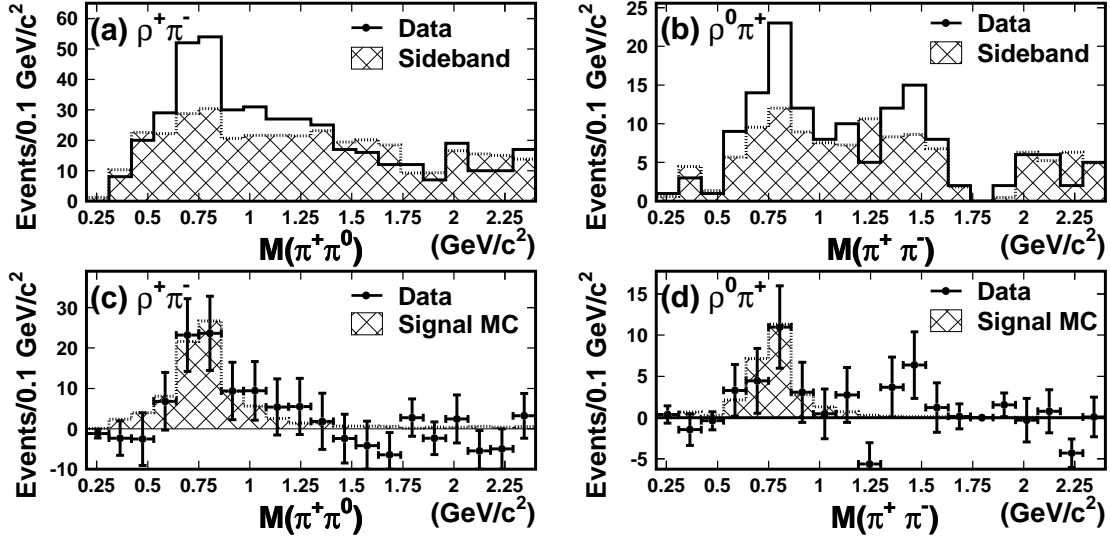


Fig. 2. The $M(\pi\pi)$ distributions for $B^0 \rightarrow \rho^\pm \pi^\mp$ (left) and $B^+ \rightarrow \rho^0 \pi^+$ (right) events in the signal region. Plots (a) and (b) show sideband events superimposed; plots (c) and (d) show the sideband subtracted plots with signal MC superimposed.

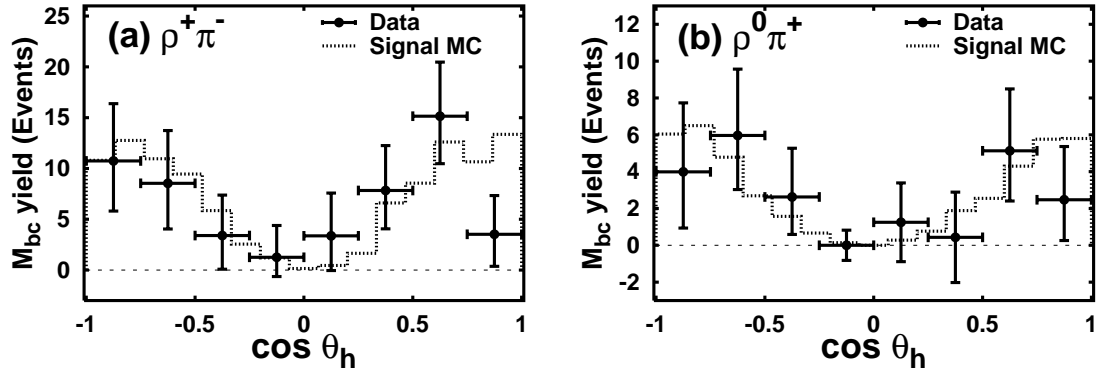


Fig. 3. The ρ meson helicity distributions for $B^0 \rightarrow \rho^\pm \pi^\mp$ (a) and $B^+ \rightarrow \rho^0 \pi^+$ (b). Signal MC distributions are shown superimposed.